Optical manipulation and study of single gold nanoparticles in solution

Ruijgrok, P.V.

4

Brownian fluctuations and heating of an optically aligned gold nanorod

Abstract – We present the first quantitative measurements of the torque exerted on a single gold nanorod in a polarized three dimensional optical trap. We determined the torque both by observing the time-averaged orientation distribution and by measuring the dynamics of the rotational Brownian fluctuations. The measurements are in good agreement with calculations, where the temperature profile around the hot nanorod gives rise to a reduced, effective viscosity. The maximum torque on a 60 nm x 25 nm nanorod was 100 pN·nm, large enough to address single-molecule processes in soft and biological matter.

The contents of this chapter have been published:
P. V. Ruijgrok, N. R. Verhart, P. Zijlstra, A. L. Tchebotareva and M. Orrit, "Brownian fluctuations and heating of an optically aligned gold nanorod", Phys. Rev. Lett. **107**, 037401 (2011)

4.1 Introduction

Since their invention some 30 years ago,[65,66] optical tweezers have become a versatile tool to study the mechanics of soft matter, investigate the statistical mechanics of model systems, and enable fabrication on the nanometer scale.[71] Rapid advances in optical trapping techniques have led to new methods by which both forces and torques can be exerted and measured. Most of those exploit the action of a polarized trap laser on an optically anisotropic microparticle.[134,135] These advances have led to a better understanding of the rotational Brownian motion of a microparticle in the laser potential,[136] and resulted in the first simultaneous measurement of torque, angle, force and position during supercoiling of DNA.[137]

Applications in environments that are structured on the nanometer scale, as found in soft matter systems, require trapping handles smaller than - or comparable in size to - the structures under study. However, optical trapping of dielectric particles below 300 nm in diameter is difficult. In contrast, the large polarizability of a metal compared to a dielectric enables the stable trapping of spherical gold nanoparticles[74] down to a diameter of 9.5 nm.[76] The optical forces that can be exerted on a metal nanoparticle have been characterized for gold and silver nanospheres[75,77,78] and gold nanorods.[79] The shape and volume of the metal nanoparticles largely determine the accessible forces, which range from 0.1 to 10 pN for gold nanorods smaller than 100 nm, i.e., relevant forces for many biophysical and soft matter systems.[70] More interestingly still, non-spherical metal nanoparticles also experience torques in optical traps, because of the anisotropy of their polarizability tensor.[80,84] Simultaneously applying a torque and a force to a metal nanoparticle would be particularly appealing for single-molecule experiments. However, no quantitative measurements of optical torques on such small particles have been published yet.

In this chapter, we demonstrate that a single gold nanorod of 25 nm in diameter and 60 nm in length can be used to exert optical torques of up to 100 pN $\cdot$ nm in a linearly polarized, three-dimensional optical trap. The restoring optical torque leads to a strong alignment of the rod, limiting the amplitude of its Brownian orientation fluctuations to about 14 degrees. In addition, we exploit the dipolar character of the rod's longitudinal plasmon resonance[138] to accurately determine the optical torque in two independent ways: (1) via the time-averaged orientation distribution deduced from white-light scattering spectra, and (2) through a dynamical analysis of rotational Brownian fluctuations observed in the polarized scattered intensity. We de-

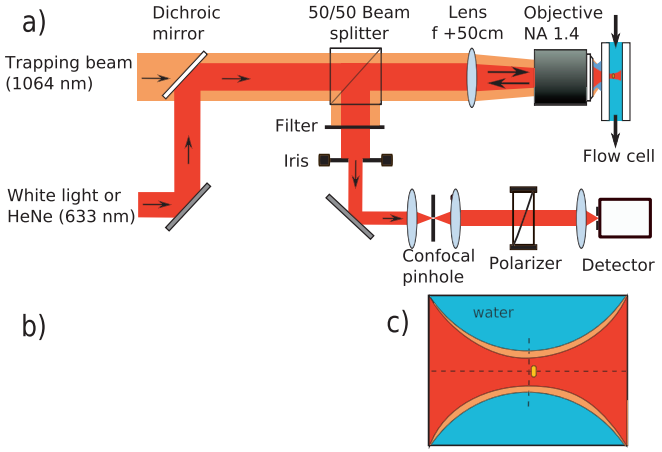

Figure 4.1: a) Scheme of the optical trap. b) Scanning electron micrograph of some gold nanorods. c) Scheme of a rod trapped in the laser focus in water. The rod is slightly shifted along the axis by radiation pressure.

termine the rod's heating by the trap beam and provide first data on the combined translational and rotational Brownian motions of a hot object in an optical trap.

4.2 Experimental Methods

The optical setup schematically shown in Fig 4.1(a) consists of a single beam optical trap at 1064 nm (5W IPG Photonics Ytterbium fiber laser). The trapping beam is focused into water about 25 μm away from the glass substrate by an objective with a high numerical aperture (Olympus oil immersion 60 x, 1.4 NA). To alleviate the spherical aberrations introduced by water's too low index, the incoming trapping beam was made slightly convergent by means of a 50 cm lens just before the objective.[118] We estimated an effective numerical aperture of 1.0 at the trap focus, see chapter 3. To obtain scattering spectra, white light from a Xenon arc lamp was focused to a spot and overlapped with the trap focus, see Fig. 4.1(c). Scattered light was collected by the focusing objective and detected by a nitrogen-cooled CCD camera coupled to a spectrograph. An iris inserted into the detection path selected the center 5 mm of the beam, to minimize depolarization effects by the objective (see Chapter 3). We inserted a 50 μm confocal pinhole at the focus of a 10 cm lens to reduce the background. Translation and rotation dynamics of the trapped rods were deduced from the back-scattered light of a HeNe laser (633 nm),

detected by a single-photon counting photodiode and analyzed with a correlation card. Gold nanorods with 60 nm average length and 25 nm average diameter, shown in the electron micrograph in Fig. 4.1(b), were synthesized by the silver-assisted seed-mediated method[119] and coated with thiolated polyethyleneglycol (mPEG, MW5000, Sigma Aldrich) to prevent their aggregation in pure water.[120] The rod suspensions were diluted with ultrapure water to limit the trapping of multiple particles during the course of a measurement, up to 2 hours.

White-light scattering spectra of a trapped nanorod are shown in Fig. 4.2(a). The parallel spectrum (analyzer along the trap polarization), displays the strong longitudinal plasmon, with maximum at 625 nm. The (nearly) Lorentzian shape of the spectrum and its narrow width (49 nm FWHM) confirm that only a single particle is trapped, see Chapter 3. With an analyzer perpendicular to the trap's polarization, the scattered signal is much weaker. Its spectrum shows residual intensity from the longitudinal plasmon at 625 nm and the transverse plasmon at about 550 nm.

4.3 Torsional stiffness quantified by the time averaged distribution of orientations

Because of the dipolar angular dependence of the scattered intensity, the time-averaged intensity $\langle I_\perp \rangle_t$ of the longitudinal plasmon observed in the perpendicular direction mainly arises from small angular fluctuations of the rod around its equilibrium orientation along the trap polarization. The intensity ratio $\langle I_\parallel \rangle_t / \langle I_\perp \rangle_t$ can be directly related to the ratio of the rotational trapping energy (or trap depth) to the thermal energy $k_B T$. The time-averaged intensities of the longitudinal plasmon in the two directions are the thermal expectation values $I_0 \langle \cos^2\theta \rangle_T$ and $I_0 \langle \sin^2\theta \cos^2\phi \rangle_T$ (θ and ϕ are the polar angles of the rod axis, see Appendix E). The probability of finding angles θ, ϕ is given by a Boltzmann distribution $\exp\left\{-U(\theta)/k_B\widetilde{T_B}\right\}$, with an effective temperature $\widetilde{T_B}$ accounting for heating by the absorbed trap light. The potential energy U is that of the rod's induced dipole in the optical field E_0, given by

$$U(\theta) = -\frac{1}{4}\mathrm{Re}\left\{\Delta\alpha\right\} E_0^2 \cos^2\theta = -\frac{1}{2}\kappa_r \cos^2\theta, \tag{4.1}$$

where $\mathrm{Re}\left\{\Delta\alpha\right\} = \mathrm{Re}\left\{\alpha_\mathrm{L} - \alpha_\mathrm{T}\right\}$ is the difference between the real parts of the longitudinal and transverse polarizabilities of the nanorod at the trap wave-

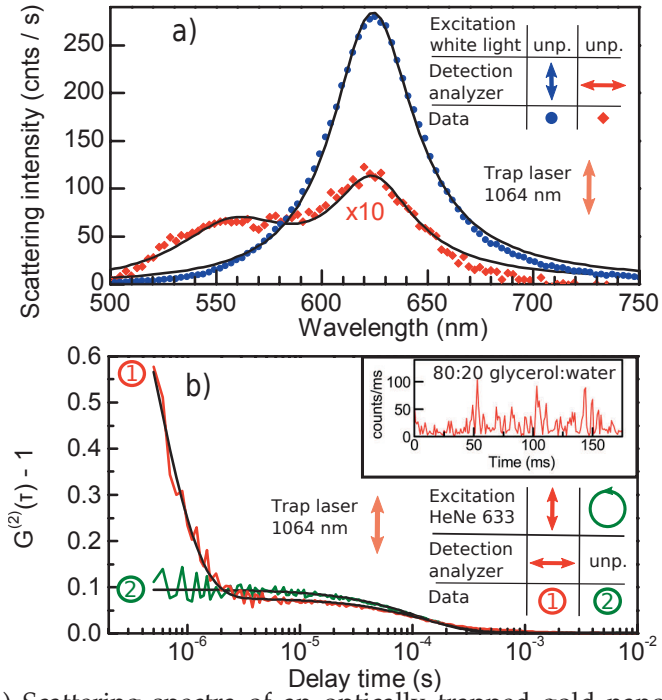

Figure 4.2: a) Scattering spectra of an optically trapped gold nanorod in water, recorded with unpolarized excitation and analyzed parallel (blue circles) or perpendicular (red diamonds) to the trap polarization. The solid lines are Lorentzian fits. Trapping power 80 mW, integration time 15 s. b) Autocorrelation functions of light from a HeNe laser, scattered by a trapped nanorod in water. Data set 1 (Red): Same nanorod as a), with an analyzer in the perpendicular direction. Data set 2 (Green): A different nanorod than a), with circularly polarized excitation and without analyzer in the detection. The solid curves are (bi-)exponential fits (characteristic times $0.48 \pm 0.01\,\mu$s and $132 \pm 8\,\mu$s for data set 1, and $96 \pm 2\ \mu$s) for data set 2. Trapping power 80 mW, acquisition time 20 s. Inset: Time trace of the intensity scattered by a rod trapped in a glycerol-water mixture, directly showing slowed down orientation fluctuations. Photon counts have been grouped in 1 ms time bins.

length, and κ_r is the rotational trap stiffness, equal to the rotational spring constant of the trap for small angles. In the limit of high rotational trap stiffness, the spectral intensity ratio is well approximated by (see Appendix E):

$$\langle I_\parallel \rangle_t / \langle I_\perp \rangle_t \simeq \kappa_r / (k_B \widetilde{T_B}) - 3. \tag{4.2}$$

A measured intensity ratio $\langle I_\parallel \rangle_t / \langle I_\perp \rangle_t = 29$ thus directly yields a trap depth $\kappa_r/2$ of 16 $k_B \widetilde{T_B}$. This corresponds to root-mean-square angular fluctuations

$\theta_{RMS} \approx \sqrt{2k_B\widetilde{T_B}/\kappa_r} = 14\,°$. The maximum torque that can be exerted is $\kappa_r/2 \approx 100$ pN · nm.

4.4 Torsional stiffness quantified by the orientational relaxation time

The angular trapping of the rod can also be characterized by the dynamics of the rotational Brownian motion. We excited the rod with a HeNe laser at 633 nm linearly polarized along the trap polarization, and detected the scattered light behind an analyzer oriented in the perpendicular direction, see Fig. 4.2(b), curve 1. As the rod wiggles around its equilibrium, the detected signal fluctuates between zero and positive values, as scattering from the transverse band and residual background are negligible. This signal is displayed in the inset of Fig. 4.2(b) for a nanorod trapped in a viscous water-glycerol mixture, where the rotational dynamics are slowed down. Fig. 4.2(b) shows the normalized autocorrelation function of the light scattered by the gold nanorod of Fig. 4.2(a), trapped in water. The correlation function is well fitted by a bi-exponential decay. We attribute the fast relaxation to rotational fluctuations of the rod in the trap. The slower relaxation is due to the transverse and axial translations of the rod in the focus, which also modulate the scattered intensity. To confirm this attribution, we recorded autocorrelation functions with circularly polarized excitation and unpolarized detection, shown in Fig. 4.2(b), data set 2. These measurements indeed present only the slow translational part, without the fast relaxation due to orientation fluctuations. In the limit of strong alignment, the rotational correlation time τ_r is half the macroscopic relaxation time of the rod in the trap, itself the ratio of the rotational friction coefficient ξ_r to the trap stiffness κ_r (see Appendix F):

$$\tau_r = \xi_r/2\kappa_r \tag{4.3}$$

where $\xi_r = \eta V C_r$, η is the viscosity of water, V the hydrodynamic volume, and C_r a geometrical factor.

4.5 Temperature dependent dynamics of Brownian fluctuations in the trap

We now correlate the time-averaged and dynamic measurements on the same particle. Whereas the time-averaged spectral ratio directly measures the com-

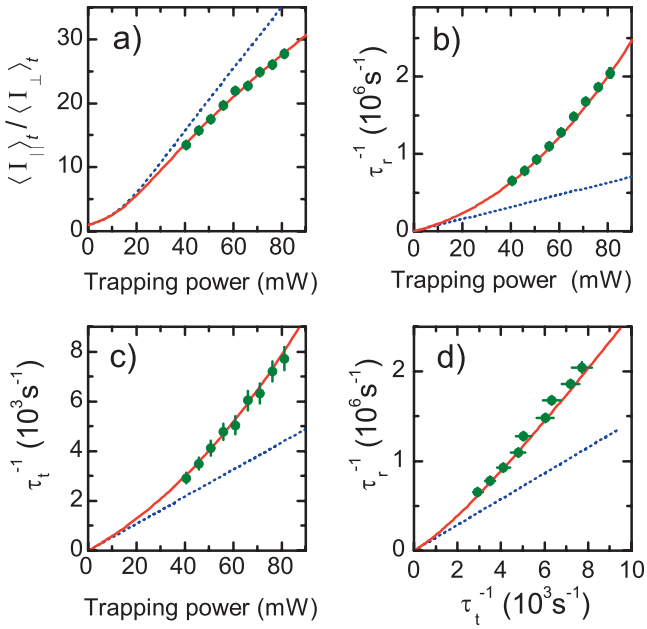

Figure 4.3: Trap characteristics as functions of trapping power, for the nanorod of figure 4.2. a) Ratio of scattered intensities of the rod's longitudinal plasmon resonance, parallel and perpendicular to the trapping laser polarization. b) Inverse of the rotation correlation time τ_r. c) Inverse of the translation correlation time τ_t. d) Inverse rotation correlation time versus inverse translation correlation time. The red lines show a global fit with an effective temperature $\widetilde{T_B}$ deduced from (a) and effective viscosities for translations $\widetilde{\eta_t}$ from (c) and rotations $\widetilde{\eta_r}$ from (b). The blue dotted lines would be observed in the complete absence of heating. In d), the blue dotted line follows from taking the same effective viscosity for rotation and translation, $\widetilde{\eta_r} = \widetilde{\eta_t}$.

petition between the trap energy and the thermal fluctuations, the rotational correlation time probes the temperature-dependent viscosity. Fig. 4.3 shows these two quantities for the same nanorod, versus trapping power. The plot of the intensity ratio $\langle I_{\parallel}\rangle_T / \langle I_{\perp}\rangle_T$ versus trap intensity in Fig. 4.3(a) shows a distinct downward curvature, which we attribute to an increase of local temperature with trap power. Indeed, the optical restoring torque on the nanorod competes with stronger thermal fluctuations as the rod gets hotter. Similarly, the plots of the inverse rotational and translational times $1/\tau_r$ and $1/\tau_t$ in Fig. 4.3(b) and Fig. 4.3(c) show an upward curvature because of the reduced water viscosity at higher trap powers.

The Brownian motion of the hot nanorod takes place in an inhomogeneous temperature- and viscosity profile. Heat diffusion being much faster

than molecular diffusion, the temperature profile accompanies the particle in its motion.[90] We describe these fluctuations phenomenologically by means of an effective temperature and of effective viscosities, as proposed recently for translational diffusion of a hot free particle.[90] This Hot Brownian Motion (HBM) has an effective temperature T_{HBM} close to the average $(T_p + T_0)/2$ between the particle temperature T_p and the bath temperature T_0, and an effective viscosity η_{HBM}. Here, we introduce another effective viscosity for the rotational HBM. This new parameter is needed because the plot of the rotational inverse time versus the translational inverse time (see Fig. 4.3(d)) is strongly nonlinear, indicating that these two effective viscosities must be different (see further data from other rods in Appendix H). Indeed, taking the same effective viscosity for both translations and rotations would lead to the straight dotted line in Fig. 4.3(d), with slope $B\kappa_r/\kappa_t$ (B depending only the shape and size of the particle under study).

To find the effective temperatures and viscosities, we globally fitted the data of Fig. 4.3 and those of two other particles measured under the same conditions to a model (see Appendix H) involving an effective temperature $\widetilde{T_B}$ and two effective viscosities $\widetilde{\eta_r}$ and $\widetilde{\eta_t}$. We adjusted the unknown parameters in the following way. The local trap intensity was obtained from the spectral intensity ratio and from the polarizability $Re\{\Delta\alpha\}$ of the three nanorods. That polarizability was calculated in the electrostatic approximation, with appropriate corrections to account for radiation damping and electron-surface scattering,[121,138] see Chapter 3. The aspect ratio of the ellipsoid and the plasmon damping rate were adjusted for each rod to reproduce the resonance wavelength and width measured in scattering spectra, see Appendix H. The intensity in the trap and the average volume of the 3 measured rods were jointly fitted to remain compatible with the volume distribution obtained from electron microscopy.

With this local intensity and the rotational times, we adjusted the rods' hydrodynamic volumes. We calculated friction coefficients from Perrin's expressions[127] for a prolate spheroid translated along the principal axes or rotated around a short principal axis, see Appendix D. The fitted effective hydrodynamic volume accounts for the PEG layer (effective thickness 5 nm[132]). The effective temperature $\widetilde{T_B}$ was fitted by the intensity ratios and found to be close to the particle's temperature T_p calculated independently from the trap intensity. The effective translational viscosity was taken as η_{HBM}, whereas the rotational effective viscosity was varied to fit the temperature dependence of rotational times in Fig. 4.3. The viscosity $\widetilde{\eta_r}$ found was close to its maximum

possible value, water's viscosity at the particle's temperature. The trap intensity found at the nanorod position was about 50% of the value expected for the focus of a diffraction-limited spot with the effective numerical aperture of 1.0 and the measured objective transmission of 19%. We attribute this low value to residual spherical aberrations.

4.6 Discussion

It is reasonable that the effective temperature $\widetilde{T_B}$ of the orientation distribution should be close to the particle's temperature T_p. Indeed, the particle should be in thermal quasi-equilibrium with the liquid shell around it. The effective translational viscosity $\widetilde{\eta_t}$ should be close to that of the Hot Brownian Motion, because our fat rod closely resembles a sphere. The difference in effective viscosities for the rotational and translational Brownian motions, however, is a surprise. Although rotations occur on much shorter times (microseconds) than translations (milliseconds), inertial effects appear too weak to explain this difference. We note that the amplitude of the rotational motion, less than 10 nm for the tip in a rotation of 20 degrees, is much smaller than the amplitude of the translational motion. The difference in viscosities may thus arise from the PEG brush, which must follow the rod's translation but not necessarily its rotation.

Our model yields a temperature increase of the rod in the trap of about 70 K at the highest trapping power of 80 mW, or about 0.9 K/mW. This value is fairly well reproduced by a simple model taking into account the fitted trap laser intensity, the calculated absorption cross section (electrostatic approximation) and heat dissipation (see Appendix H). Similar heating rates were previously found for gold spheres.[77,88] Such temperature rises may be of concern for certain applications. However, the temperature around the nanorod decays rapidly with distance, with a characteristic length of the order of the particle's radius. At a distance 100 nm away from the rod, the temperature increase is only about 10 degrees (See Appendix G) for the highest trapping power used here.

4.7 Conclusions

We have determined for the first time the torque that can be exerted on a single gold nanorod in a polarized optical trap. The maximum torque we measured was 100 pN·nm, large enough to address typical single-molecule

processes.[137] The small volume of a single gold nanorod compared to conventional dielectric particles paves the way to study environments which exhibit mechanical heterogeneity on nanometer length scales.